

VLTI/VINCI diameter constraints on the evolutionary status of δ Eri, ξ Hya, η Boo

F. Thévenin¹, P. Kervella², B. Pichon¹, P. Morel¹, E. Di Folco³, and Y. Lebreton⁴

¹ Laboratoire Cassiopée, UMR 6202 CNRS, Observatoire de la Côte d’Azur, BP 4229, 06304 Nice Cedex 4, France

² Laboratoire d’Études Spatiales et d’Instrumentation Astrophysique (LESIA), UMR 8109 du CNRS, Observatoire de Paris, Section de Meudon, 5 place Jules Janssen, 92195 Meudon Cedex, France

³ European Southern Observatory, Karl-Schwarzschild Strasse 2, 85748 Garching, Germany

⁴ GEPI, UMR 8111 CNRS, Observatoire de Paris, Section de Meudon, 5 place Jules Janssen, 92195 Meudon Cedex, France

Received 27 September 2004 / Accepted 16 January 2005

Abstract. Using VLTI/VINCI angular diameter measurements, we constrain the evolutionary status of three asteroseismic targets: the stars δ Eri, ξ Hya, η Boo. Our predictions of the mean large frequency spacing of these stars are in agreement with published observational estimations. Looking without success for a companion of δ Eri, we doubt its classification as an RS CVn star.

Key words. stars: evolution – stars: fundamental parameters – techniques: interferometric

1. Introduction

After two years of operation, the commissioning instrument VINCI of the VLTI has provided valuable stellar diameter measurements. Among the impact of these diameters are the studies of main sequence stars, where diameters combined with asteroseismic frequencies can be used to constrain evolutionary status and mass. Several papers have been published (Ségransan et al. 2003; Kervella et al. 2003a,b; 2004a; Di Folco et al. 2004) with important results on stellar fundamental parameters prior to the use of the dedicated VLTI light combiner AMBER (Petrov et al. 2003). The aim of the present paper is to complete previous studies using VINCI to measure the diameter of three subgiant and giant stars that are among selected asteroseismic targets for ground-based observations and space missions: δ Eri, ξ Hya, η Boo. We perform a preliminary study of their evolutionary status by constraining their mass, their helium content and their age. One of the purposes of this paper is to show that in the future, the use of stellar diameters will be a significant constraint for evolutionary models for given input physics. We first describe the characteristics of each of the three stars (Sect. 2) and then we present diameter measurements (Sect. 3) for each star. We construct evolutionary models satisfying spectro-photometric observable constraints and we compare asteroseismic large frequencies with measured ones. We present these models (Sect. 4) and we draw some conclusions on the classification and fundamental parameters of the three stars.

2. Global characteristics of the stars

The first part of Table 1 presents the observational data of the three stars. The second part of this table summarizes some input parameters and output data of the models.

2.1. δ Eri

δ Eri (HD 23249, HR 1136, HIP 17378) has been thoroughly studied by photometry and spectroscopy and is classified as a K0 IV star (Keenan & Pitts 1980). It belongs to the group of the nearest stars with an accurate Hipparcos parallax of 110.58 ± 0.88 mas (Perryman et al. 1997). The star has been classified as a weakly active and X-ray soft source (Huensch et al. 1999) after a lengthy search for its activity. Wilson & Bappu (1957) concluded that the possible detection of emission in the H&K lines is “*exceedingly weak*” – so weak that it is questionable. It took more than 20 years to inconclusively detect its activity with Copernicus, revealing a weak emission in MgII (Weiler & Oegerle 1979). Fisher et al. (1983) tried to detect a periodic variation in the photometric data and concluded that, if it exists, the amplitude is below ± 0.02 mag with a period of 10 days. They suggested that δ Eri could be classified as an RS CVn star. An RS CVn is defined as a F-G binary star having a period shorter than 14 days, with chromospheric activity and with a period of rotation synchronized with its orbital period (Linsky 1984), giving the star high rotational velocity inducing strong activity. This is in contrast with the low level

Table 1. Observable characteristics of the stars and best model reproducing them. The subscripts “_{ini}” and “_{surf}” respectively refer to initial values and current surface quantities. Note that the presented errors of VLTI/VINCI angular diameters are the statistical ones followed by the systematical ones. Note also that D/D_\odot is equal to R/R_\odot .

	δ Eri	ξ Hya	η Boo			
V	3.51 ± 0.02	3.54 ± 0.01	2.68 ± 0.01			
BC	-0.24 ± 0.01	-0.26 ± 0.01	-0.06 ± 0.01			
$T_{\text{eff}}(\text{K})$	5074 ± 60	5010 ± 100	6050 ± 150			
L/L_\odot	3.19 ± 0.06	60.7 ± 4.1	8.95 ± 0.20			
$[\text{Fe}/\text{H}]_{\text{surf}}$	0.13 ± 0.08	-0.04 ± 0.12	0.24 ± 0.07			
$\log g$	3.77 ± 0.16	2.93 ± 0.30	3.66 ± 0.20			
$\theta_{\text{LD}}(\text{mas})$	2.394 ± 0.014 ± 0.025	2.386 ± 0.009 ± 0.019	2.200 ± 0.027 ± 0.016			
D/D_\odot	2.33 ± 0.03	10.3 ± 0.3	2.68 ± 0.05			
$\pi(\text{mas})$	110.58 ± 0.88	25.23 ± 0.83	88.17 ± 0.75			
$\Delta\nu_0(\mu\text{Hz})$	43.8 ± 0.3	7.1	40.47 ± 0.05			

	δ Eri diffusion	δ Eri no diffusion	ξ Hya diffusion	ξ Hya no diffusion	η Boo diffusion	η Boo no diffusion
M/M_\odot	1.215	1.215	2.65	2.65	1.70	1.70
Age of the ZAMS (Myr)	20.14	20.06	2.724	2.719	12.68	12.67
Age (from ZAMS) (Myr)	6194.	6196.	509.52	505.34	2738.5	2355.
Y_{ini}	0.28	0.28	0.275	0.275	0.260	0.260
$[Z/X]_{\text{ini}}$	0.148	0.148	0.00	0.00	0.367	0.367
$T_{\text{eff}}(\text{K})$	5055.	5066.	5037.	5034.	6050.	6090.
L/L_\odot	3.176	3.230	61.23	61.0	8.944	8.978
R/R_\odot	2.328	2.337	10.30	10.30	2.728	2.697
$\log g$	3.788	3.785	2.835	2.832	3.796	3.806
Y_{surf}	0.266	0.28	0.274	0.275	0.228	0.260
$[Z/X]_{\text{surf}}$	0.123	0.148	0.00	0.00	0.303	0.367
$M_{\text{CZ}}(M_\star)$	0.729	0.727	0.608	0.596	0.9994	0.9994
$R_{\text{CZ}}(R_\star)$	0.475	0.475	0.422	0.417	0.8388	0.8505
$\Delta\nu_0(\mu\text{Hz})$	45.27	44.91	7.23	7.28	41.91	42.47

of activity detected for δ Eri making doubtful its classification as an RS CVn star. δ Eri has a projected rotational velocity of $v \sin i = 1.0 \text{ km s}^{-1}$ (de Meideros & Mayor 1999) and the hypothetical RS CVn classification forces us to conclude that the binary is seen pole-on therefore explaining the lack of photometric variation and also of any variation of the radial velocity (Santos et al. 2004). To reveal the presence of a close companion around δ Eri, we set several VLTI/VINCI observations at different baselines (see Sect. 3).

We estimate its bolometric luminosity $L_\star/L_\odot = 3.19 \pm 0.06$ using the Alonso et al. (1999) empirical bolometric corrections (BC, $\text{BC} = -0.24 \pm 0.01$ for giants, this is the dominant source of uncertainty on the luminosity). We adopt the Santos et al. (2004) values for the effective temperature $T_{\text{eff}} = 5074 \pm 60 \text{ K}$, logarithmic surface gravity $\log g = 3.77 \pm 0.16$ and surface iron abundance $[\text{Fe}/\text{H}] = 0.13 \pm 0.03$. These parameters are different from – but within the error bars of – the parameters proposed by Pijpers (2003) for this star, except the metallicity which is 0.24 dex higher. Bouchy & Carrier (2003) have measured a mean large frequency spacing of $43.8 \mu\text{Hz}$ that we will try to reproduce with our model. We recall that the large frequency spacing is defined as the difference between frequencies of

modes with consecutive radial order n : $\Delta\nu_l(n) = \nu_{n,l} - \nu_{n-1,l}$. In the high frequency range, i.e. large radial orders, $\Delta\nu_l(n)$ is almost constant with a mean value strongly related to the square root of the mean density of the star. To obtain the mean large frequency separation, we average over $l = 0-2$.

2.2. ξ Hya

ξ Hya (HD 100407, HR 4450, HIP 56343) is a giant star (G7 III) which has been considered by Eggen (1977) as a spurious member of the Hyades group because it departs slightly from the regression line of giant stars in the colour diagrams ($b - y$, $R - I$) and (M_1 , $R - I$) of that stellar group.

Its Hipparcos parallax is $25.23 \pm 0.83 \text{ mas}$. We estimate its bolometric luminosity $L_\star/L_\odot = 60.7 \pm 4.1$ using BC ($\text{BC} = -0.26 \pm 0.01$) from Alonso et al. (1999). We adopt the spectroscopic parameters derived by Mc William (1990): effective temperature $T_{\text{eff}} = 5010 \pm 100 \text{ K}$, $\log g = 2.93 \pm 0.30$ and $[\text{Fe}/\text{H}] = -0.04 \pm 0.12$. These parameters are different from – but within the error bars of – the parameters adopted by Frandsen et al. (2002) for this star. The star belongs to the HR diagram at the lowest part of the giant branch

corresponding to an evolved star with a mass around $3 M_{\odot}$. Using a set of CORALIE spectra, Frandsen et al. (2002) detected solar-like oscillations suggesting radial modes with the largest amplitudes almost equidistant around $7.1 \mu\text{Hz}$. That important detection opens the possibility of better constraining the model of this star for which the mass is not well-known.

2.3. η Boo

η Boo (HD 121370, HR 5235, HIP 67927) is a subgiant (G0 IV) spectroscopic binary (SB1) studied recently by Di Mauro et al. (2003, 2004) and Guenther (2004). Its Hipparcos parallax is 88.17 ± 0.75 mas. Having large overabundances of Si, Na, S, Ni and Fe, it has been considered as super-metal-rich by Feltzing & Gonzales (2001). We adopt here a luminosity $L_{\star}/L_{\odot} = 8.95 \pm 0.20$ using BC (BC = -0.06 ± 0.01 , this is the dominant source of uncertainty on the luminosity) from Vandenberg & Clem (2003) for this subgiant, with an effective temperature $T_{\text{eff}} = 6050 \pm 150$ K representing the average of five effective temperature determinations in the [Fe/H] catalogue of Cayrel de Strobel et al. (2001) and the spectroscopic $\log g = 3.66 \pm 0.20$ and [Fe/H] = 0.24 ± 0.07 from Feltzing & Gonzales (2001). These parameters are different from – but within the error bars of – the parameters adopted by Di Mauro et al. (2003, 2004) for this star. Asteroseismic observations of δ Eri have been reported by Carrier et al. (2005) with $\Delta\nu_0 = 39.9 \pm 0.1 \mu\text{Hz}$ and by Kjeldsen et al. (2003) with $\Delta\nu_0 = 40.47 \pm 0.05 \mu\text{Hz}$.

3. Diameter interferometric measurements

3.1. VINCI and the VLTI

The European Southern Observatory's Very Large Telescope Interferometer (Glindemann et al. 2000) has been operated on top of the Cerro Paranal, in Northern Chile since March 2001. For the observations reported in this work, the light coming from two telescopes (two 0.35 m test siderostats or VLT/UT1-UT3) was combined coherently in VINCI, the VLT Interferometer Commissioning Instrument (Kervella et al. 2000). We used a regular K band filter ($\lambda = 2.0\text{--}2.4 \mu\text{m}$) for these observations.

3.2. Data reduction

We used an improved version of the standard VINCI data reduction pipeline (Kervella et al. 2004b), whose general principle is based on the original FLUOR algorithm (Coudé du Foresto et al. 1997). The two calibrated output interferograms are subtracted to remove residual photometric fluctuations. Instead of the classical Fourier analysis, we implemented a time-frequency analysis (Ségransan et al. 1999) based on a continuous wavelet transform.

The atmospheric piston effect between the two telescopes corrupts the amplitude and the shape of the fringe peak in the wavelet power spectrum. As described in Kervella et al. (2004b), the properties of the fringe peaks in the time and frequency domains are monitored automatically, in order to reject from the processing the interferograms that are strongly

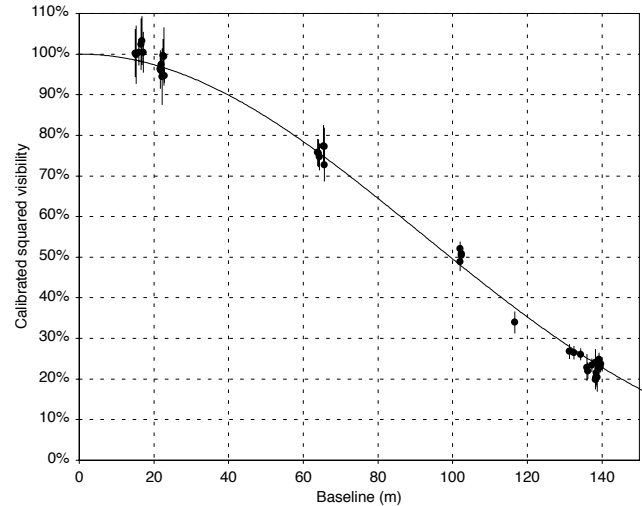


Fig. 1. Squared visibility measurements obtained on δ Eri. The solid line is a limb darkened disk model with $\theta_{\text{LD}} = 2.394 \pm 0.014 \pm 0.025$ mas (statistical and systematic errors).

affected by the atmospheric piston. This selection reduces the statistical dispersion of the squared coherence factors (μ^2) measurement, and avoids biases from corrupted interferograms. The final μ^2 values are derived by integrating the average wavelet power spectral density (PSD) of the interferograms at the position and frequency of the fringes. The residual photon and detector noise backgrounds are removed using a linear least squares fit of the PSD at high and low frequency. The statistical error bars on μ^2 are computed from the series of μ^2 values obtained on each target star (typically a few hundred interferograms) using the bootstrapping technique.

3.3. Measured visibilities and angular diameters

The visibility values obtained on δ Eri, ξ Hya and η Boo are listed in Tables 2 to 5, and plotted in Figs. 1 to 3.

The calibration of the visibilities obtained on δ Eri and η Boo was done using well-known calibrator stars that were selected from the Cohen et al. (1999) catalogue. The uniform disk (UD) angular diameter of these stars was converted into a limb darkened value and then to a K band uniform disk angular diameter using the recent non-linear law coefficients taken from Claret et al. (2000). As demonstrated by Bordé et al. (2002), the star diameters in this list have been measured very homogeneously to a relative precision of approximately 1%.

The VINCI instrument has no spectral dispersion and its bandpass corresponds to the K band filter ($2\text{--}2.4 \mu\text{m}$). It is thus important to compute the precise effective wavelength of the instrument in order to determine the angular resolution at which we are observing the targets. The effective wavelength differs from the filter mean wavelength because of the detector quantum efficiency curve, the fiber beam combiner transmission and the object spectrum. It is only weakly variable as a function of the spectral type.

To derive the effective wavelength of our observations, we computed a model taking into account the star spectrum and the VLTI transmission. The instrumental transmission of VINCI

Table 2. δ Eri squared visibilities.

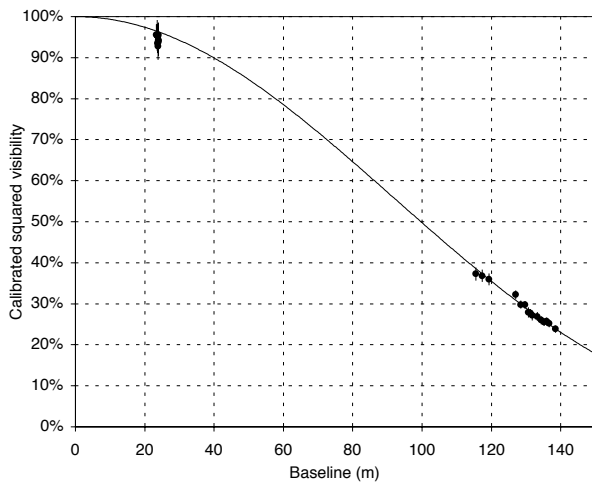
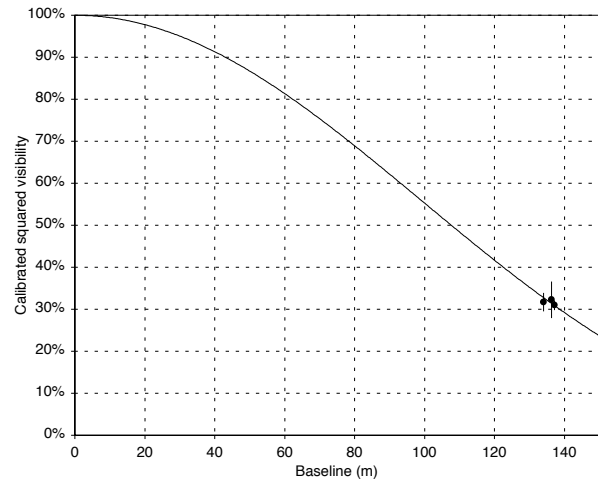
Julian Date	Stations	N	B (m)	Az. (deg)	$V^2 \pm \text{stat} \pm \text{syst}$	Calibrator
2 452 682.528	B3-D1	74	22.638	14.95	$0.9941 \pm 0.0712 \pm 0.0014$	δ Lep
2 452 682.541	B3-D1	460	21.963	14.63	$0.9740 \pm 0.0140 \pm 0.0014$	δ Lep
2 452 682.545	B3-D1	281	21.735	14.55	$0.9639 \pm 0.0264 \pm 0.0014$	δ Lep
2 452 682.607	B3-D1	140	16.514	14.78	$1.0242 \pm 0.0632 \pm 0.0014$	δ Lep
2 452 682.612	B3-D1	340	15.954	14.99	$1.0045 \pm 0.0321 \pm 0.0014$	δ Lep
2 452 682.618	B3-D1	133	15.285	15.27	$0.9987 \pm 0.0715 \pm 0.0013$	δ Lep
2 452 671.562	B3-D1	233	22.437	14.84	$0.9960 \pm 0.0409 \pm 0.0031$	δ Lep
2 452 671.567	B3-D1	95	22.164	14.71	$0.9442 \pm 0.0697 \pm 0.0029$	δ Lep
2 452 671.574	B3-D1	210	21.749	14.55	$0.9623 \pm 0.0474 \pm 0.0030$	δ Lep
2 452 671.631	B3-D1	397	17.152	14.59	$1.0042 \pm 0.0501 \pm 0.0014$	δ Lep
2 452 671.635	B3-D1	206	16.756	14.71	$1.0331 \pm 0.0604 \pm 0.0014$	δ Lep
2 452 671.651	B3-D1	237	14.947	15.44	$1.0023 \pm 0.0588 \pm 0.0014$	δ Lep
2 452 672.553	B3-D1	401	22.756	15.02	$0.9465 \pm 0.0164 \pm 0.0014$	δ Lep
2 452 672.567	B3-D1	426	22.013	14.65	$0.9585 \pm 0.0153 \pm 0.0014$	δ Lep
2 452 672.603	B3-D1	379	19.478	14.26	$0.9911 \pm 0.0235 \pm 0.0014$	δ Lep
2 452 672.607	B3-D1	237	19.086	14.28	$1.0134 \pm 0.0540 \pm 0.0015$	δ Lep
2 452 673.567	B3-D1	236	21.898	14.60	$0.9780 \pm 0.0322 \pm 0.0014$	δ Lep
2 452 673.579	B3-D1	264	21.130	14.39	$0.9940 \pm 0.0264 \pm 0.0015$	δ Lep
2 452 673.609	B3-D1	441	18.693	14.31	$1.0197 \pm 0.0253 \pm 0.0015$	δ Lep
2 452 674.527	B3-D1	262	23.527	15.78	$0.9718 \pm 0.0294 \pm 0.0014$	δ Lep
2 452 674.557	B3-D1	415	22.253	14.75	$0.9757 \pm 0.0241 \pm 0.0015$	δ Lep
2 452 674.562	B3-D1	405	22.003	14.64	$0.9833 \pm 0.0249 \pm 0.0015$	δ Lep
2 452 674.566	B3-D1	314	21.756	14.55	$0.9778 \pm 0.0281 \pm 0.0015$	δ Lep
2 452 675.547	B3-D1	432	22.640	14.95	$0.9731 \pm 0.0213 \pm 0.0014$	δ Lep
2 452 676.557	B3-D1	383	21.997	14.64	$0.9674 \pm 0.0203 \pm 0.0014$	δ Lep
2 452 676.561	B3-D1	402	21.734	14.55	$0.9813 \pm 0.0201 \pm 0.0015$	δ Lep
2 452 676.565	B3-D1	259	21.474	14.47	$0.9678 \pm 0.0338 \pm 0.0014$	δ Lep
2 452 676.590	B3-D1	447	19.612	14.26	$0.9883 \pm 0.0227 \pm 0.0014$	δ Lep
2 452 676.602	B3-D1	328	18.603	14.32	$0.9453 \pm 0.0318 \pm 0.0013$	δ Lep
2 452 677.543	B3-D1	480	22.582	14.92	$0.9651 \pm 0.0283 \pm 0.0014$	δ Lep
2 452 677.547	B3-D1	445	22.366	14.80	$0.9695 \pm 0.0294 \pm 0.0014$	δ Lep
2 452 677.551	B3-D1	256	22.137	14.70	$0.9283 \pm 0.0407 \pm 0.0013$	δ Lep
2 452 677.587	B3-D1	267	19.633	14.26	$1.0093 \pm 0.0407 \pm 0.0015$	δ Lep
2 452 677.598	B3-D1	381	18.695	14.31	$1.0013 \pm 0.0384 \pm 0.0015$	δ Lep
2 452 677.603	B3-D1	287	18.286	14.36	$1.0432 \pm 0.0455 \pm 0.0015$	δ Lep
2 452 678.537	B3-D1	230	22.746	15.02	$1.0024 \pm 0.0382 \pm 0.0014$	δ Lep
2 452 678.548	B3-D1	121	22.186	14.72	$0.9746 \pm 0.0520 \pm 0.0014$	δ Lep
2 452 678.559	B3-D1	168	21.531	14.49	$0.9900 \pm 0.0492 \pm 0.0014$	δ Lep
2 452 678.584	B3-D1	422	19.649	14.26	$1.0167 \pm 0.0354 \pm 0.0011$	δ Lep
2 452 678.593	B3-D1	150	18.893	14.29	$1.0966 \pm 0.0618 \pm 0.0012$	δ Lep
2 452 679.561	B3-D1	402	21.184	14.40	$0.9800 \pm 0.0353 \pm 0.0014$	δ Lep
2 452 679.566	B3-D1	278	20.892	14.35	$1.0211 \pm 0.0435 \pm 0.0015$	δ Lep
2 452 683.578	B3-D1	374	19.065	14.28	$0.9596 \pm 0.0152 \pm 0.0012$	δ Lep
2 452 683.582	B3-D1	449	18.708	14.31	$0.9900 \pm 0.0147 \pm 0.0013$	δ Lep
2 452 683.586	B3-D1	283	18.316	14.36	$0.9378 \pm 0.0232 \pm 0.0012$	δ Lep
2 452 683.593	B3-D1	269	17.654	14.48	$0.9915 \pm 0.0274 \pm 0.0013$	δ Lep
2 452 683.598	B3-D1	250	17.167	14.59	$0.9693 \pm 0.0290 \pm 0.0012$	δ Lep
2 452 683.602	B3-D1	261	16.783	14.70	$0.9154 \pm 0.0274 \pm 0.0012$	δ Lep
2 452 684.516	B3-D1	296	22.937	15.15	$0.9431 \pm 0.0287 \pm 0.0014$	δ Lep
2 452 684.527	B3-D1	400	22.396	14.82	$0.9473 \pm 0.0220 \pm 0.0014$	δ Lep
2 452 684.562	B3-D1	439	20.148	14.27	$0.9859 \pm 0.0225 \pm 0.0013$	δ Lep
2 452 684.579	B3-D1	415	18.747	14.30	$0.9882 \pm 0.0232 \pm 0.0013$	δ Lep
2 452 685.587	B3-D1	206	17.669	14.47	$1.0318 \pm 0.0277 \pm 0.0013$	δ Lep

and the VLTI was first modeled taking into account all known effects and then calibrated based on several bright reference star observations with the UTs (see Kervella et al. 2003b, for details).

Taking the weighted average wavelength of this model spectrum gives an effective wavelength of $\lambda_{\text{eff}} = 2.178 \pm 0.003 \mu\text{m}$ for δ Eri, ξ Hya and η Boo. The visibility fits were computed taking into account the limb darkening of the stellar

Table 3. δ Eri squared visibilities (continued from Table 2).

Julian Date	Stations	N	B (m)	Az. (deg)	$V^2 \pm \text{stat} \pm \text{syst}$	Calibrator
2 452 524.854	E0-G1	350	65.689	307.62	$0.7271 \pm 0.0400 \pm 0.0054$	70 Aql, 31 Ori
2 452 524.858	E0-G1	336	65.583	307.23	$0.7720 \pm 0.0464 \pm 0.0057$	70 Aql, 31 Ori
2 452 524.863	E0-G1	239	65.450	306.79	$0.7729 \pm 0.0521 \pm 0.0057$	70 Aql, 31 Ori
2 452 524.890	E0-G1	452	64.342	303.74	$0.7467 \pm 0.0329 \pm 0.0055$	70 Aql, 31 Ori
2 452 524.895	E0-G1	456	64.115	303.16	$0.7561 \pm 0.0336 \pm 0.0056$	70 Aql, 31 Ori
2 452 524.899	E0-G1	452	63.877	302.56	$0.7579 \pm 0.0332 \pm 0.0056$	70 Aql, 31 Ori
2 452 555.889	B3-M0	312	132.444	27.46	$0.2742 \pm 0.0150 \pm 0.0055$	δ Phe
2 452 555.893	B3-M0	275	131.275	27.44	$0.2769 \pm 0.0168 \pm 0.0056$	δ Phe
2 452 556.810	B3-M0	200	139.144	30.60	$0.2477 \pm 0.0152 \pm 0.0067$	δ Phe
2 452 556.817	B3-M0	395	139.500	30.10	$0.2294 \pm 0.0113 \pm 0.0062$	δ Phe
2 452 556.822	B3-M0	373	139.635	29.80	$0.2370 \pm 0.0117 \pm 0.0064$	δ Phe
2 452 564.830	B3-M0	146	138.416	28.23	$0.2047 \pm 0.0228 \pm 0.0019$	HR 8685
2 452 567.762	B3-M0	236	137.272	32.21	$0.2245 \pm 0.0153 \pm 0.0044$	HR 8685
2 452 577.789	B3-M0	173	138.926	28.46	$0.2248 \pm 0.0314 \pm 0.0070$	45 Eri, HR 2549
2 452 577.794	B3-M0	187	138.426	28.23	$0.2156 \pm 0.0289 \pm 0.0067$	45 Eri, HR 2549
2 452 213.776	UT1-UT3	73	101.996	232.98	$0.4883 \pm 0.0203 \pm 0.0102$	χ Phe
2 452 213.777	UT1-UT3	332	102.056	232.83	$0.5207 \pm 0.0138 \pm 0.0109$	χ Phe
2 452 213.791	UT1-UT3	69	102.374	231.76	$0.5089 \pm 0.0172 \pm 0.0106$	χ Phe
2 452 213.793	UT1-UT3	312	102.394	231.65	$0.5044 \pm 0.0150 \pm 0.0105$	χ Phe
2 452 578.723	B3-M0	269	135.965	33.09	$0.2393 \pm 0.0257 \pm 0.0063$	τ Cet
2 452 578.740	B3-M0	169	138.202	31.51	$0.2520 \pm 0.0246 \pm 0.0066$	τ Cet
2 452 578.745	B3-M0	74	138.752	31.02	$0.2133 \pm 0.0307 \pm 0.0056$	τ Cet
2 452 585.799	B3-M0	298	134.322	27.55	$0.2608 \pm 0.0134 \pm 0.0071$	τ Cet
2 452 601.810	B3-M0	206	116.676	28.41	$0.3674 \pm 0.0290 \pm 0.0082$	τ Cet
2 452 602.728	B3-M0	123	138.193	28.15	$0.2183 \pm 0.0241 \pm 0.0056$	τ Cet
2 452 602.742	B3-M0	396	136.193	27.73	$0.2412 \pm 0.0174 \pm 0.0062$	τ Cet

**Fig. 2.** Squared visibility measurements obtained on ξ Hya. The solid line is a limb darkened disk model with $\theta_{LD} = 2.386 \pm 0.009 \pm 0.019$ mas (statistical and systematic errors).**Fig. 3.** Squared visibility measurements obtained on η Boo. The solid line is a limb darkened disk model with $\theta_{LD} = 2.200 \pm 0.027 \pm 0.016$ mas (statistical and systematic errors).

disk of each stars. We used power law intensity profiles derived from the limb darkening models of Claret (2000) in the K band.

The resulting limb darkened diameters for the three program stars are given in Table 1. The statistical error bars were computed from the statistical dispersion of the series of μ^2 values obtained on each star (typically a few hundred), using the bootstrapping technique. The systematic error bars come from the uncertainties on the angular diameters of the calibrators that

were used for the observation. They impact the precision of the interferometric transfer function measurement, and thus affect the final visibility value. Naturally, these calibration error bars do not get smaller when the number of observations increases, as the statistical errors do. The detailed methods and hypothesis used to compute these error bars are given in Kervella et al. (2004b).

Table 4. ξ Hya squared visibilities.

Julian Date	Stations	N	B (m)	Az. (deg)	$V^2 \pm \text{stat} \pm \text{syst}$	Calibrators
2452 681.743	B3-D1	333	23.650	27.39	$0.9539 \pm 0.0376 \pm 0.0008$	α Crt
2452 681.747	B3-D1	460	23.727	26.48	$0.9520 \pm 0.0305 \pm 0.0008$	α Crt
2452 681.751	B3-D1	343	23.801	25.51	$0.9281 \pm 0.0334 \pm 0.0007$	α Crt
2452 681.777	B3-D1	452	23.995	20.50	$0.9555 \pm 0.0304 \pm 0.0008$	α Crt
2452 681.781	B3-D1	332	23.989	19.60	$0.9383 \pm 0.0337 \pm 0.0008$	α Crt
2452 681.785	B3-D1	427	23.975	18.89	$0.9424 \pm 0.0305 \pm 0.0008$	α Crt
2452 682.729	B3-D1	354	23.407	29.82	$0.9560 \pm 0.0251 \pm 0.0009$	α Crt
2452 682.752	B3-D1	295	23.846	24.85	$0.9519 \pm 0.0280 \pm 0.0009$	α Crt
2452 682.792	B3-D1	297	23.904	17.19	$0.9420 \pm 0.0317 \pm 0.0007$	α Crt
2452 682.801	B3-D1	403	23.773	15.47	$0.9351 \pm 0.0237 \pm 0.0007$	α Crt
2452 760.583	B3-M0	350	138.521	60.37	$0.2383 \pm 0.0058 \pm 0.0069$	α Crt
2452 760.600	B3-M0	343	136.690	63.11	$0.2520 \pm 0.0061 \pm 0.0073$	α Crt
2452 760.605	B3-M0	391	135.918	63.96	$0.2568 \pm 0.0059 \pm 0.0075$	α Crt
2452 760.635	B3-M0	433	129.762	68.49	$0.2971 \pm 0.0058 \pm 0.0077$	α Crt
2452 760.640	B3-M0	388	128.458	69.20	$0.2978 \pm 0.0061 \pm 0.0077$	α Crt
2452 760.645	B3-M0	284	127.037	69.92	$0.3221 \pm 0.0071 \pm 0.0084$	α Crt
2452 761.624	B3-M0	429	131.833	67.24	$0.2714 \pm 0.0063 \pm 0.0097$	51 Hya
2452 761.628	B3-M0	303	130.716	67.94	$0.2787 \pm 0.0077 \pm 0.0100$	51 Hya
2452 761.665	B3-M0	421	119.296	73.16	$0.3592 \pm 0.0063 \pm 0.0131$	51 Hya
2452 761.671	B3-M0	402	117.300	73.87	$0.3681 \pm 0.0067 \pm 0.0135$	51 Hya
2452 761.675	B3-M0	340	115.485	74.49	$0.3727 \pm 0.0087 \pm 0.0136$	51 Hya
2452 762.604	B3-M0	470	135.192	64.66	$0.2554 \pm 0.0021 \pm 0.0092$	51 Hya
2452 762.609	B3-M0	454	134.296	65.44	$0.2600 \pm 0.0022 \pm 0.0094$	51 Hya
2452 762.614	B3-M0	386	133.310	66.21	$0.2689 \pm 0.0049 \pm 0.0097$	51 Hya
2452 762.623	B3-M0	441	131.274	67.59	$0.2771 \pm 0.0027 \pm 0.0100$	51 Hya

Table 5. η Boo squared visibilities.

Julian Date	Stations	N	B (m)	Az. (deg)	$V^2 \pm \text{stat} \pm \text{syst}$	Calibrators
2452 760.684	B3-M0	131	134.046	64.22	$0.3167 \pm 0.0187 \pm 0.0119$	α Crt
2452 760.696	B3-M0	50	136.318	63.31	$0.3227 \pm 0.0415 \pm 0.0121$	α Crt
2452 763.693	B3-M0	187	137.132	62.88	$0.3095 \pm 0.0092 \pm 0.0064$	μ Vir

3.4. Search for a companion to δ Eri

δ Eri is classified as an RS CVn variable (Kholopov et al. 1998), and has shown a small amplitude photometric variability ($m_V = 3.51$ to 3.56). Fisher et al. (1983) have also reported photometric variations with an amplitude $\Delta m_V = 0.02$ over a period of 10 days. This small amplitude and the apparent absence of periodic radial velocity modulation lead these authors to propose that δ Eri is a close binary star seen nearly pole on ($i \leq 5$ deg). Following this idea, we can suggest three hypotheses to explain the observed photometric variations:

1. The main star is ellipsoidal. This would result in a modulation of its projected surface along the line of sight during its rotation. This deformation would be caused by the close gravitational interaction of the main star with the unseen companion.
2. The companion creates a hot spot on the hemisphere of the main star that is facing it. It is changing in apparent surface when the system rotates, probably synchronously.
3. The pole of the main component has a dark spot that changes in apparent surface during the rotation of the star.

The period of the photometric variations, if attributed to the presence of an orbiting companion, allows us to deduce the

distance between the two components through Kepler's third law. At the distance of δ Eri, this corresponds to an angular separation of approximately 9 mas, easily resolvable using the moderately long baselines of the VLTI. Using the B3-D1 stations of the VLTI, we have taken advantage of the fact that the azimuth of the projected baseline is almost constant for observations of δ Eri to monitor the evolution of its visibility over a period of 13 nights. The projected length is also very well suited to the expected separation. Our interferometric data (Fig. 4) does not show any systematic deviation from the uniform disk model fit obtained using the longer baselines, at a level of $0.2 \pm 0.3\%$, consistent with zero. From these measurements, we conclude that no companion is detected at a level of about $\pm 2\%$ of the luminosity of the primary star. This result is consistent with the fact that δ Eri does not deviate significantly from the surface-brightness relations determined by Kervella et al. (2004c).

4. Models and results

In order to obtain a rapid estimate of the improvements brought by the new interferometric constraints on the radius on the determination of the mass and age of the three stars, we have

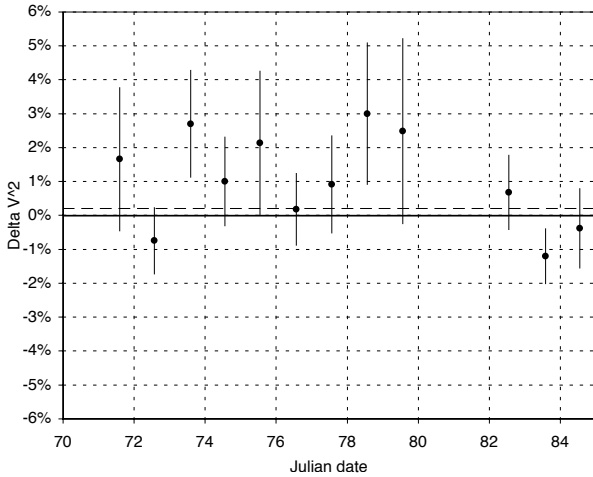


Fig. 4. Observed deviation of the squared visibilities of δ Eri (B3-D1 baseline only) with respect to the visibility model of a $\theta_{\text{UD}} = 2.394$ mas uniform disk model. The dashed line represents the average deviation over all observations (0.21%).

calculated evolutionary stellar models that we compare to observations. In these models we have adopted a given set of standard input physics and the observational parameters described in Sect. 2 and Table 1. We do not intend to examine in detail the effects on the uncertainties of the details of the models (envelope, convection, overshooting or other extra mixing) on the results presented here.

The parameters used to construct our CESAM (Morel 1997) evolutionary models are summarized in Table 1. The convection is described by Canuto & Mazitelli's theory (1991, 1992) and the atmospheres are restored on the basis of Kurucz's atlas models (1992). The other input physics are identical to those adopted for the star Procyon (see Kervella et al. 2004a). The adopted metallicity Z/X , which is an input parameter for the evolutionary computations, is given by the iron abundance measured in the atmosphere with the help of the following approximation: $\log\left(\frac{Z}{X}\right) \approx [\text{Fe}/\text{H}] + \log\left(\frac{Z}{X}\right)_{\odot}$. We use the solar mixture of Grevesse & Noels (1993): $\left(\frac{Z}{X}\right)_{\odot} = 0.0245$.

The evolutionary tracks are initialized at the Pre-Main Sequence stage. Note that the age is counted from the ZAMS. In CESAM, the ZAMS is defined as the stage of the end of the Pre-Main Sequence where the gravitational energy release is equal to the nuclear one. We have computed models with and without microscopic diffusion of chemical species.

To fit observational data (effective temperature T_{eff} , luminosity L and surface metallicity $[Z/X]_{\text{surf}}$) with corresponding results of various computations, we adjust the main stellar modeling parameters: mass, age and metallicity. In figures representing the zoom of HR diagram (Figs. 6, 8, 10 and 12), the (rectangular) error boxes are derived from the values and accuracies of the stellar parameters quoted in Table 1. The present (new) values of radii, presented in this paper, select sub-areas in these error boxes and hence the new measures of diameters are used to discriminate between our models (see Table 1). Our best model is the one that satisfies first the luminosity and radius constraint and second the effective temperature constraint. On the zooms of the HR diagrams (see Figs. 6, 8, 10 and 12),

the measured radius and its confidence interval appear as diagonal lines. We notice that the addition of the radius measurement reduces significantly the uncertainty domain, and in some cases tightens the allowed range for ages by a factor of three (see below). We have computed models that include overshooting of the convective core (radius R_{co}) over the distance $O_v = A_{\text{ov}} \min(H_p, R_{\text{co}})$ where R_{co} is the core radius, following the prescriptions of Schaller et al. (1992).

4.1. δ Eri

First, we adopt an initial helium content similar to the Sun, $Y_{\text{ini}} = 0.28$ and $[Z/X]_{\text{ini}} = 0.148$, both stars having similar ages and abundances (this will be confirmed hereafter).

Then, with mass and metallicity as free parameters, we have computed a grid of evolutionary tracks in order to reproduce observational data. Our best model without diffusion and without overshooting gives $M = 1.215 M_{\odot}$ and an age (from the ZAMS) of 6196 Myr. Our best model with diffusion and an overshooting value of $A_{\text{ov}} = 0.15$ in agreement with the results of Ribas et al. (2000) gives $M = 1.215 M_{\odot}$, an age (from the ZAMS) of 6194 Myr and a diameter of $D = 2.328 D_{\odot}$. See Figs. 5 and 6.

The mean large frequency splitting found for our best model is $45.27 \mu\text{Hz}$. This result is in agreement within two per cent with the value of $43.8 \mu\text{Hz}$ of the mean large frequency splitting reported by Carrier et al. (2003).

4.2. ξ Hya

We have computed a grid of evolutionary tracks (with and without diffusion) in order to reproduce observational data. Hence, we derived the following parameters: $M = 2.65 M_{\odot}$, $Y_{\text{ini}} = 0.275$ and $[Z/X]_{\text{ini}} \equiv 0.0$. Our best model with diffusion and an overshooting value of $A_{\text{ov}} = 0.20$ in agreement with the results of Ribas et al. (2000) gives us an age (from the ZAMS) of 509.5 Myr and a diameter of $D = 10.3 D_{\odot}$. To improve the modeling, a better precision of the diameter is required as it is the case for the two other stars discussed in this paper, for which the accuracy is better by an order of magnitude. See Figs. 7 and 8.

Solar-like oscillations of that star were discovered by Frandsen et al. (2002) with a mean spacing of $7.1 \mu\text{Hz}$; see also Teixeira et al. (2003). From our model, we computed a value of $7.2 \mu\text{Hz}$ similar to the theoretical value presented by Frandsen et al. or Teixeira et al.

4.3. η Boo

Concerning the values of T_{eff} and its corresponding uncertainty, we have chosen conservative values based upon various determinations: Feltzing & Gonzales (2001) gives $T_{\text{eff}} = 6000 \pm 100$ K whereas Cayrel de Strobel (2001) gives a range between 5943 and 6219 K. We notice that DiMauro et al. adopt $T_{\text{eff}} = 6028 \pm 45$ K but in our study, we take advantage of the constraint given by the new diameter value which reduces the uncertainty as shown in Figs. 10 or 12.

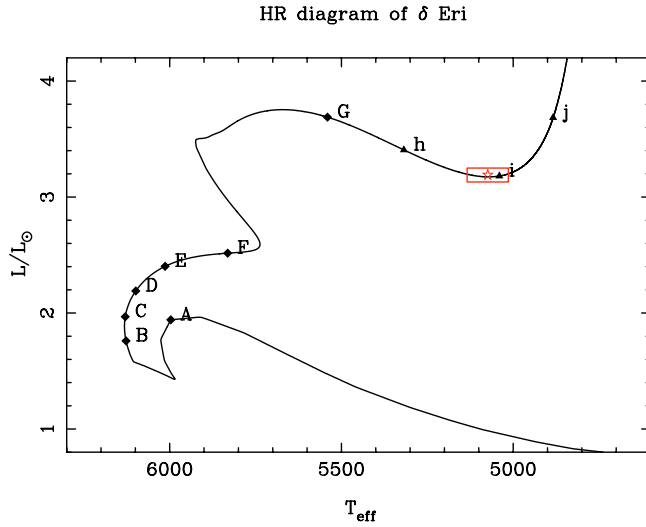


Fig. 5. Evolutionary tracks in the H-R diagram for δ Eri from label “A” (0 Myr) to label “G” (6000 Myr), shown by upper case letters and squares with time steps of 1000 Myr; from label “h” (6100 Myr) to label “j” (6300 Myr), shown by lower case letters and triangles with time steps of 100 Myr.

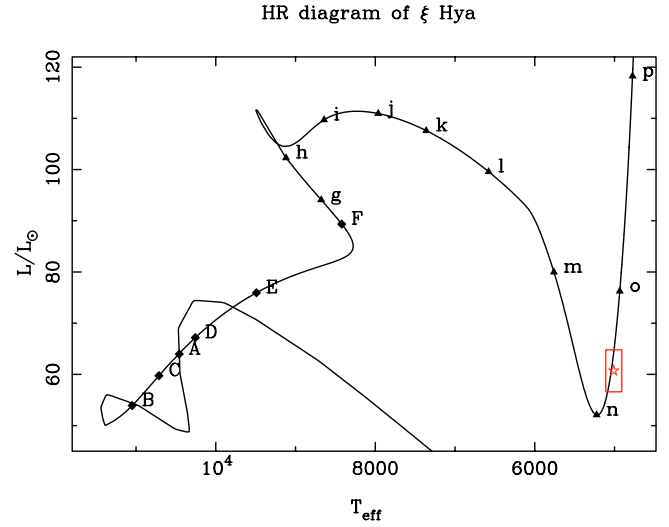


Fig. 7. Evolutionary tracks in the H-R diagram for ξ Hya from label “A” (0 Myr) to “F” (500 Myr), shown by upper case letters and squares with time steps of 100 Myr; from label “g” (502 Myr) to “p” (511 Myr), shown by lower case letters and triangles with time steps of 1 Myr.

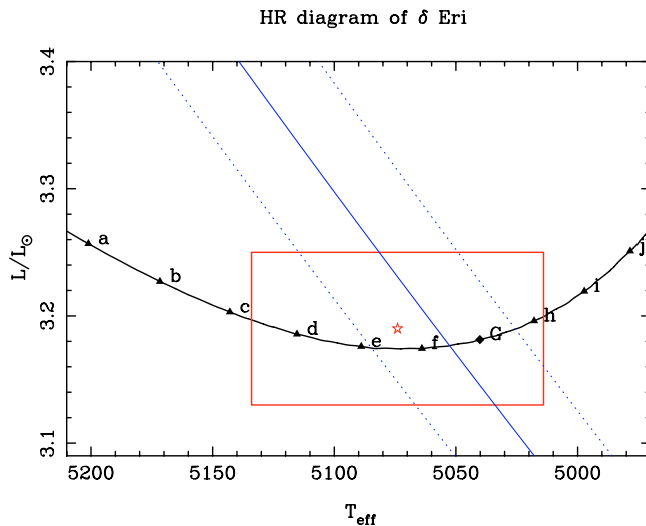


Fig. 6. Zoom of the evolutionary tracks in the H-R diagram for δ Eri from label “a” (6140 Myr) to label “j” (6230 Myr), shown by lower case letters and triangles with time steps of 10 Myr (except label “G” at 6200 Myr shown by an upper case letter and a square). Our best model is close to label “f” at 6194 Myr (see Table 1).

In a first attempt to characterize this star, DiMauro et al. (2003) limit the range of mass between $1.64 M_{\odot}$ and $1.75 M_{\odot}$. Guenther (2004) adopted in his conclusion a mass of $1.706 M_{\odot}$ with an initial chemical composition: $X_{\text{ini}} = 0.71$, $Y_{\text{ini}} = 0.25$ and $Z_{\text{ini}} = 0.04$. In the present study, we have computed a grid of models and it appears that the best fitting parameters are $M = 1.70 M_{\odot}$ with an initial chemical composition $X_{\text{ini}} = 0.70$, $Y_{\text{ini}} = 0.26$ and $Z_{\text{ini}} = 0.04$. A first set of models have been computed with the simplest available reliable physics (and therefore without diffusion, as probably done by the previously cited authors). A second set of models have also been computed with improved physics. Thus, we include

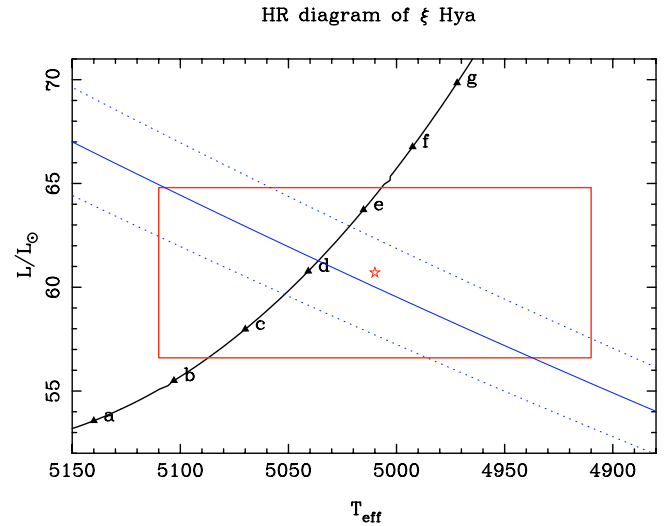


Fig. 8. Zoom of the evolutionary tracks in the H-R diagram for ξ Hya from label “a” (509.2 Myr) to “g” (509.8 Myr), shown by lower case letters and triangles with time steps of 0.1 Myr. Our best model is close to label “d” at 509.5 Myr (see Table 1).

convective overshooting (with $A_{\text{ov}} = 0.15$, see previous discussion), diffusion and radiative diffusivity (see Morel & Thévenin 2002) which controls diffusion of chemical elements in intermediate mass stars. The two sets of results give similar results except for the ages: the age of the best model with diffusion (2738.5 Myr) is higher than the age of the best model without diffusion (2355.0 Myr).

As shown, for example, in Fig. 10, without the constraint given by the diameter, the age would range from 2295 Myr (between label “b” and label “c”) to 2410 Myr (close to label “n”), with a derived uncertainty of 115 Myr. For a given set of input physics, the constraint on diameter reduces the uncertainty on the age by about a factor of three: the age would

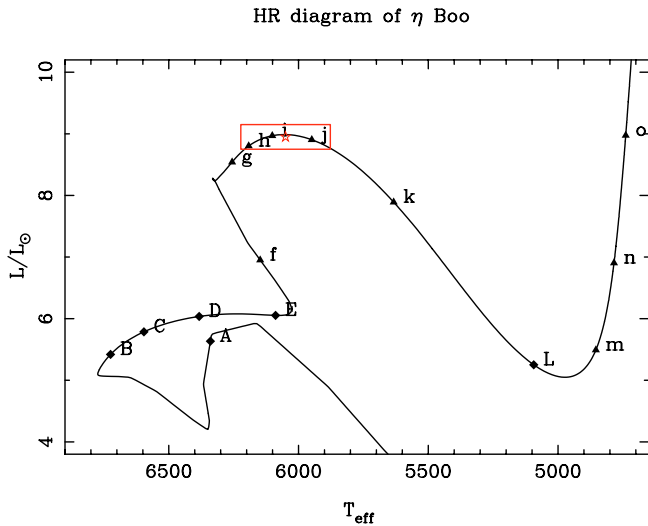


Fig. 9. Evolutionary tracks in the H-R diagram for η Boo (model without diffusion) from label “A” (0 Myr) to “E” (2000 Myr), shown by upper case letters and squares with time steps of 500 Myr; from label “f” (2200 Myr) to “o” (2650 Myr), shown by lower case letters and triangles with time steps of 50 Myr (except label “L” at 2500 Myr shown by an upper case letter and a square).

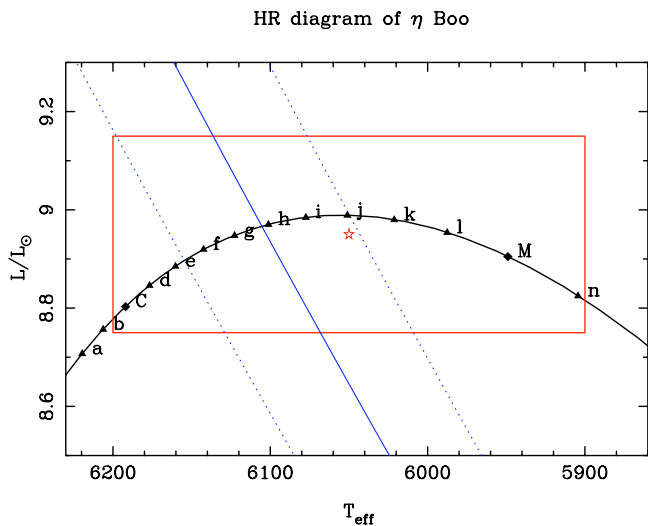


Fig. 10. Zoom of the evolutionary tracks in the H-R diagram for η Boo (model without diffusion) from label “a” (2280 Myr) to “n” (2744 Myr), shown by lower case letters and triangles with time steps of 10 Myr (except labels “C” at 2300 Myr and label “M” a 2400 Myr shown by an upper case letters and squares). Our best model is close to label “h” at 2350 Myr (see Table 1).

be ranging from 2323 Myr (close to label “e”) to 2370 Myr (close to label “j”), corresponding to a (reduced) uncertainty of 47 Myr (Figs. 9–12). Note that our model for η Boo with diffusion (Figs. 11 and 12) has the star in a very short-lived phase of evolution (which is, of course, possible but with a small, but non zero, probability).

5. Concluding remarks

We have measured with the instrument VLTI/VINCI the angular diameters of three subgiant and giant stars and used them

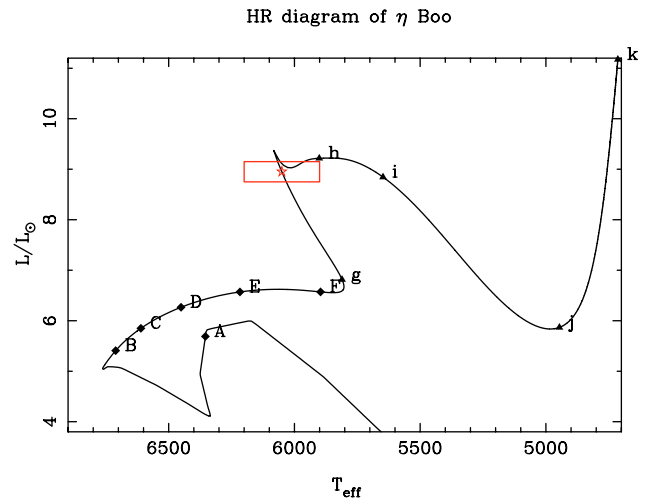


Fig. 11. Evolutionary tracks in the H-R diagram for η Boo (model with diffusion) from label “A” (0 Myr) to label “F” (2500 Myr), shown by upper case letters and squares with a time step of 500 Myr; label “g” at 2700 Myr shown by a triangle; from label “h” (2750 Myr) to label “k” (2900 Myr), shown by lower case letters and triangles with a time step of 50 Myr.

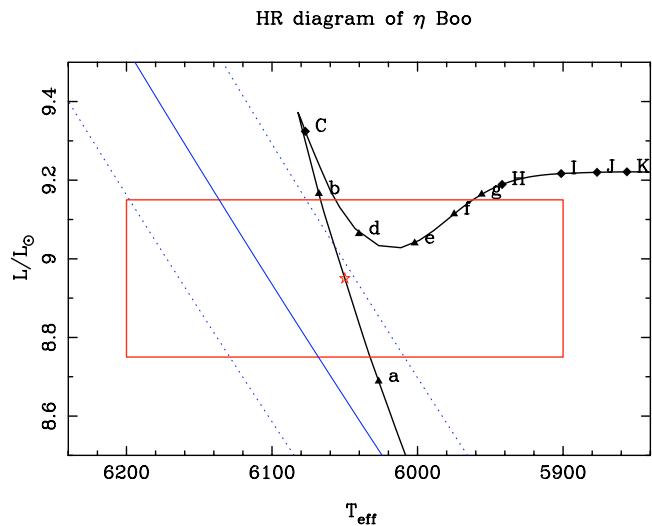


Fig. 12. Zoom of the evolutionary tracks in the H-R diagram for η Boo (model with diffusion) from label “a” (2738 Myr) to label “g” (2745 Myr), shown by lower case letters and triangles with time steps of 1 Myr (except label “C” at 2740 Myr shown by a square); from label “H” (2745 Myr) to label “K” (2760 Myr), shown by upper case letters and squares with time steps of 5 Myr. Our best model is between label “a” (at 2738 Myr) and label “b” (at 2739 Myr) (see Table 1).

as an additive constraint to the spectro-photometric and asteroseismic ones to perform a study of the stellar evolutionary status.

Owing the position of the three stars in the HR diagram, the determination of the modeling parameters, in particular the age, is very sensitive to the input physics, due to the rapidity of the stellar evolution compared to the size of the error boxes.

With our input physics and observational constraints, δ Eri is a star at the end of the subgiant phase ($M = 1.215 M_{\odot}$) with an age of 6.2 Gyr. We attempt without success to detect a close

companion forcing us to conclude that the classification of δ Eri as an RS CVn star is doubtful.

ξ Hya has been constrained with success with a model adopting a mass of $2.65 M_{\odot}$ and an age of 510 Myr.

η Boo is a subgiant slightly more evolved than Procyon with a similar age of 2.7 Gyr. With a mass of at $M = 1.7 M_{\odot}$ (similar to the mass adopted by Di Mauro et al. 2003), we were able to reproduce the VLTI/VINCI radius. We notice that because of the short evolutionary time scales of a model crossing rather large error boxes, the results of the models – in particular the age – are very sensitive to the input physics (for instance, the core mixing. Some progress in the asteroseismic observations is now required to better constrain the evolutionary state of giant stars for which the frequency spacings (Bouchy & Carrier 2003; Bedding & Kjeldsen 2003) are still relatively imprecise. The improvement of the angular diameter estimations in the future will further tighten the uncertainty domain in the HR diagram, especially as detailed modeling of the atmosphere will be required. This improvement will naturally require a higher precision on the parallax value to derive the linear diameters.

Acknowledgements. The VINCI public commissioning data reported in this paper has been retrieved from the ESO/ST-ECF Archive. The VINCI pipeline includes the wavelets processing technique, developed by D. Ségransan (Obs. de Genève). No VLTI observation would have been possible without the efforts of the ESO VLTI team, to whom we are grateful. This work has been performed using the computing facilities provided by the program Simulations Interactives et Visualisation en Astronomie et Mécanique (SIVAM) at the computer center of the Observatoire de la Côte d'Azur. This research has made use of the Simbad database operated at CDS, Strasbourg, France. We thank the referee, T. R. Bedding, for his suggested improvements of this paper.

References

- Alonso, A., Arribas, S., & Martínez-Roger, C. 1999, *A&AS*, 140, 261
 Bedding, T. R., & Kjeldsen, H. 2003, *PASA*, 20, 203
 Bordé, P., Coudé du Foresto, V., Chagnon, G., & Perrin, G. 2002, *A&A*, 393, 183
 Bouchy, F., & Carrier, F. 2003, *Ap&SS*, 284, 21
 Canuto, V. M., & Mazitelli, I. 1991, *ApJ*, 370, 295
 Canuto, V. M., & Mazitelli, I. 1992, *ApJ*, 389, 729
 Carrier, F., Bouchy, F., & Eggenberger, P. 2003, in *Asteroseismology across the HR diagram*, ed. M. J. Thompson, M. S., Cunha, & M. J. Monteiro (Kluwer Academic Publishers) 311
 Carrier, F., Eggenberger, P., & Bouchy, F. 2005, *A&A*, 434, 1085
 Cayrel de Strobel, G., Soubiran, C., & Ralite, N. 2001, *A&A*, 373, 159
 Claret, A. 2000, *A&A*, 363, 1081
 Cohen, M., Walker, R. G., Carter, B., et al. 1999, *AJ*, 117, 1864
 Coudé du Foresto, V., Ridgway, S., & Mariotti, J.-M. 1997, *A&AS*, 121, 379
 Di Folco, E., Thévenin, F., Kervella, P., et al. 2004, *A&A*, 426, 601
 Di Mauro, M. P., Christensen-Dalsgaard, J., Kjeldsen, H., Bedding, T. R., & Paternò, L. 2003, *A&A*, 404, 341
 Di Mauro, M. P., Christensen-Dalsgaard, J., Paternò, L., & D'Antona, F. 2004, *Sol. Phys.*, 220, 185
 Eggen O. J., *ApJ*, 215, 812
 Feltzing, S., & Gonzales, G. 2001, *A&A*, 367, 251
 Fisher, G. F., Hall, D. S., Henry, G. W., et al. 1983, *IBVS*, 2259, 1
 Frandsen, S., Carrier, F., Aerts, C., et al. 2002, *A&A*, 394, L5
 Glindemann, A., Abuter, R., Carbognani, F., et al. 2000, *SPIE*, 4006, 2
 Grevesse, N., & Noels, A. 1993, *Cosmic Abundances of the Elements, in Origin and Evolution of the Elements*, ed. N. Prantzos, E. Vangioni-Flam, & M. Cassé (Cambridge University Press), 14
 Guenther, D. B. 2004, *ApJ*, 612, 454
 Huensch, M., Schmitt, J. H. M. M., & Voges, W. 1999, *A&AS*, 132, 155
 Keenan, P. C., & Pitts, R. E. 1980, *ApJS*, 42, 541
 Kervella, P., Coudé du Foresto, V., Glindemann, A., & Hofmann, R. 2000, *SPIE*, 4006, 31
 Kervella, P., Thévenin, F., Ségransan, D., et al. 2003a, *A&A*, 404, 1087
 Kervella, P., Thévenin, F., Morel, P., Bordé, P., & Di Folco, E. 2003b, *A&A*, 408, 681
 Kervella, P., Thévenin, F., Morel, P., et al. 2004a, *A&A*, 413, 251
 Kervella, P., Ségransan, D., & Coudé du Foresto, V. 2004b, *A&A*, 425, 1161
 Kervella, P., Thévenin, F., Ségransan, D., & Di Folco, E. 2004c, *A&A*, 426, 297
 Kholopov, P. N., et al., *The Combined General Catalogue of Variable Stars*, 1998, 4th Edition
 Kjeldsen, H., Bedding, T. R., Baldry, I. K., et al. 2003, *AJ*, 126, 1483
 Kurucz, R. L. 1992, *The Stellar Populations of Galaxies*, *IAU Symp.*, 149, 225
 Linsky, J. L. 1984, *LNP*, 193, 244
 McWilliam, A. 1990, *ApJS*, 74, 1075
 de Medeiros, J., & Mayor, M. 1999, *A&AS*, 139, 433
 Morel, P. 1997, *A&AS*, 124, 597
 Morel, P., & Thévenin, F. 2002, *A&A*, 390, 611
 Perryman, M. A. C., Lindegren, L., Kovalevsky, J., et al. 1997, *A&A*, 323, 49
 Petrov, R., Amber consortium 2003, *EAS Pub. Series*, 6, 111
 Pijpers, F. P. 2003, *A&A*, 400, 241
 Ribas, I., Jordi, C., & Giménez, À. 2000, *MNRAS*, 318, L55
 Santos, N. C., Israelian, G., & Mayor, M. 2004, *A&A*, 415, 1153
 Schaller, G., Schaerer, D., Meynet, G., & Maeder, A. 1992, *A&AS*, 96, 269
 Ségransan, D., Forveille, T., Millan-Gabet, C. P. R., & Traub, W. A. 1999, in *ASP Conf. Ser.*, 194, 290
 Ségransan, D., Kervella, P., Forveille, T., & Queloz, D. 2003, *A&A*, 397, L5
 Teixeira, T. C., Christensen-Dalsgaard, J., Carrier, F., et al. 2003, *Ap&SS*, 284, 233
 Vandenberg, D. A., & Clem, J. L. 2003, *AJ*, 126, 778
 Weiler, E. J., & Oegerle, W. R. 1979, *ApJS*, 39, 537
 Wilson, O. C., & Vainu Bappu, M. K. 1957, *ApJ*, 125, 661